UCRL-JRNL-229340

The 4He Total Photo-Absorption Cross Section With Two- Plus Three-Nucleon Interactions From Chiral Effective Field Theory

S. Quaglioni, P. Navratil

March 23, 2007

Physics Letters B

The ^{4}He total photo-absorption cross section with two- plus three-nucleon interactions from chiral effective field theory

Sofia Quaglioni and Petr Navrátil
Lawrence Livermore National Laboratory, P.O. Box 808, L-414, Livermore, CA 94551, USA
(Dated: March 10, 2007)

The total photo-absorption cross section of ^{4}He is evaluated microscopically using two- (NN) and three-nucleon (NNN) interactions based upon chiral effective field theory (χEFT). The calculation is performed using the Lorentz integral transform method along with the *ab initio* no-core shell model approach. An important feature of the present study is the consistency of the NN and NNN interactions and also, through the Siegert theorem, of the two- and three-body current operators. This is due to the application of the χEFT framework. The inclusion of the NNN interaction produces a suppression of the peak height and enhancement of the tail of the cross section. We compare to calculations obtained using other interactions and to representative experiments. The rather confused experimental situation in the giant resonance region prevents discrimination among different interaction models.

Interactions among nucleons are governed by quantum chromodynamics (QCD). In the low-energy regime relevant to nuclear structure and reactions, this theory is non-perturbative, and, therefore, hard to solve. Thus, theory has been forced to resort to models for the interaction, which have limited physical basis. New theoretical developments, however, allow us connect QCD with low-energy nuclear physics. Chiral effective field theory (χEFT) [1, 2] provides a promising bridge to the underlying theory, QCD. Beginning with the pionic or the nucleon-pion system [3] one works consistently with systems of increasing number of nucleons [4]. One makes use of spontaneous breaking of chiral symmetry to systematically expand the strong interaction in terms of a generic small momentum and takes the explicit breaking of chiral symmetry into account by expanding in the pion mass. Nuclear interactions are non-perturbative, because diagrams with purely nucleonic intermediate states are enhanced [1, 2]. Therefore, the chiral perturbation expansion is performed for the potential. The χEFT predicts, along with the nucleon-nucleon (NN) interaction at the leading order, a three-nucleon (NNN) interaction at the next-to-next-to-leading order or N^{2}LO [2, 5, 6], and even a four-nucleon (NNNN) interaction at the fourth order (N^{3}LO) [7]. The details of QCD dynamics are contained in parameters, low-energy constants (LEC's), not fixed by the symmetry, but can be constrained by experiment. At present, high-quality NN potentials have been determined at N^{3}LO [8]. A crucial feature of χEFT is the consistency between the NN, NNN and NNNN parts. As a consequence, at N^{2}LO and N^{3}LO, except for two parameters assigned to two NNN diagrams, the potential is fully constrained by the parameters defining the NN interaction. The full interaction up to N^{2}LO was first applied to the analysis of *nd* scattering [6] and later the N^{3}LO NN potential was combined with the available NNN at N^{2}LO to study the ^{7}Li structure [9]. In a recent work [10] the NN potential at N^{3}LO of Ref. [8] and the NNN interaction at N^{2}LO [5, 6] have been applied to the calculation of various properties of *s*- and mid-*p*-shell nuclei, using the *ab initio* no-core shell model (NCSM) [11, 12], up to now the only approach able to handle the chiral NN+NNN potentials for systems beyond $A = 4$. In that study, a preferred choice of the two NNN LEC's was found and the fundamental importance of the chiral NNN interaction was demonstrated for reproducing the structure of light nuclei. In the present work, we apply for the first time the same χEFT interactions to the *ab inito* calculation of reaction observables involving the continuum of the four-nucleon system. In particular, we study the ^{4}He total photo-absorption cross section.

Experimental measurements of the α particle photodisintegration suffer from a recurrent history of large discrepancies in the near-threshold region, where the ^{4}He$(\gamma,p)^3$H and the ^{4}He$(\gamma,n)^3$He break-up channels dominate the total photo-absorption cross section (we refer the reader to the reviews of available data made in Refs. [13–15]). The latest examples date back to the past two years [15, 16]. Of particular controversy is the height of the cross section at the peak, alternatively found to be either pronounced or suppressed with up to 100% relative difference between different experimental data. With the exception of [17], early evaluations of the ^{4}He photodisintegration [14, 18, 19] showed better agreement with the high-peaked experiments, and, ultimately, with those of Ref. [16]. The inability of these calculations to reproduce a suppressed cross section at low energy was often imputed to the semi-realistic nature of the Hamiltonian and, in particular, to the absence of NNN forces. The introduction of NNN interactions leads, indeed, to a reduction of the peak height, as it was recently shown in a calculation of the photo-absorption cross section with the Argonne V18 (AV18) NN potential augmented by the Urbana IX (UIX) NNN force. A similar effect has also been found using the phase-equivalent non-local counterpart of AV18 derived through the unitary correlation operator method (UCOM). In both cases, however, the suppression is not sufficient to reach the low-lying data, and in particular those of Ref. [15]. The latter calculations represent a substantial step forward in the study of the ^{4}He photo-disintegration. However, they still present a residual degree of arbitrariness in the choice of the NNN force

to complement AV18 in the first case, or in the choice of the unitary transformation leading to the non-local phase-equivalent interaction in the second case. As an example, the Illinois potential models have been found to be more realistic NNN partners of AV18 in the reproduction of the structure of light p-shell nuclei [20]. It is therefore important to calculate the ^{4}He photo-absorption cross section in the framework of χEFT theory, where NN and NNN potentials are derived in a consistent way and their relative strengths is well established by the order in the chiral expansion.

When the wavelength of the incident radiation is much larger than the spatial extension of the system under consideration, the nuclear photo-absorption process can be described in good approximation by the cross section

$$\sigma_\gamma(\omega) = 4\pi^2 \frac{e^2}{\hbar c} \omega R(\omega) \ , \qquad (1)$$

where ω is the incident photon energy and the inclusive response function

$$R(\omega) = \int d\Psi_f \left| \langle \Psi_f | \hat{D} | \Psi_0 \rangle \right|^2 \delta(E_f - E_0 - \omega) \qquad (2)$$

is the sum of all the transitions from the ground state $|\Psi_0\rangle$ to the various allowed final states $|\Psi_f\rangle$ induced by the dipole operator:

$$\hat{D} = \sqrt{\frac{4\pi}{3}} \sum_{i=1}^{A} \frac{\tau_i^z}{2} r_i Y_{10}(\hat{r}_i) \ . \qquad (3)$$

In the above equations ground- and final-state energies are denoted by E_0 and E_f, respectively, whereas τ_i^z and $\vec{r}_i = r_i \hat{r}_i$ represent the isospin third component and center of mass frame coordinate of the ith nucleon. This form of the transition operator includes the leading effects of the meson-exchange currents through the Siegert's theorem. Additional contributions to the cross section (due to retardation, higher electric multiples, magnetic multiples) not considered by this approximation are found to be negligible in the $A = 2$ [21] and $A = 3$ [22] nuclei, in particular for $\omega \lesssim 40$ MeV. A similar behavior can be expected from a system of small dimensions like the ^{4}He.

Denoting with $\hat{H}$ the full Hamiltonian of the system,

$$\hat{H} = \frac{1}{A} \sum_{i<j}^{A} \frac{\vec{p}_i - \vec{p}_j}{2m} + \sum_{i<j}^{A} V_{ij}^{\rm NN} + \sum_{i<j<k}^{A} V_{ijk}^{\rm NNN} \ , \qquad (4)$$

where m is the nucleon mass, V_{ij}^{NN} is the sum of N^{3}LO NN and Coulomb interactions, and V_{ij}^{NNN} is the N^{2}LO NNN force, we i) solve the many-body Schrödinger equation for the ground state $|\Psi_0\rangle$, ii) obtain the response (2) by evaluation [23, 24] and subsequent inversion [**?**] of an integral transform with a Lorentzian kernel of finite width $\sigma_I \sim 10{-}20$ MeV ($z = E_0 + \sigma_R + i\sigma_I$),

$$L(\sigma_R, \sigma_I) \ = \ -\frac{1}{\sigma_I} {\rm Im} \left\{ \langle \psi_0 | \hat{D}^\dagger \frac{1}{z - \hat{H}} \hat{D} | \psi_0 \rangle \right\} \qquad (5)$$

$$= \ \int R(\omega) \frac{1}{(\omega - \sigma_R)^2 + \sigma_I^2} \, d\omega \ , \qquad (6)$$

and iii) calculate the photo-absorption cross section in the long wave-length approximation using Eq. (1). Following the above mentioned steps, a fully microscopic result for the ^{4}He photo-absorption cross section can be reached through the use of efficient expansions over localized many-body states. Indeed, in the technique summarized by Eqs. (5-6) and known as Lorentz integral transform (LIT) method [26], the continuum problem is mapped onto a bound-state-like problem.

The present calculations are performed in the framework of the *ab initio* NCSM approach [11]. This method looks for the eigenvectors of $\hat{H}$ in form of expansions over a complete set of harmonic oscillator (HO) basis states up to a maximum excitation of $N_{max}\hbar\Omega$ above the minimum energy configuration , where Ω is the HO parameter. The convergence to the exact results with increasing N_{max} is accelerated by the use of an effective interaction derived, in this case, from the adopted NN and NNN χEFT potentials at the three-body cluster level [12]. The reliability of the NCSM approach combined with the LIT method was recently validated by comparing to the results obtained with the effective-interaction hyper-spherical harmonics (EIHH) technique [27] in a recent benchmark calculation [28]. A complete description of the NCSM approach was presented , e.g., in Refs. [11, 12]. Here, we emphasize some of the aspects involved in a calculation of the effective interaction at the the three-body cluster level in presence of a NNN potential. We use a Jacobi coordinate HO basis antisymmentrized according to the method described in Ref. [29] The NCSM calculation proceeds in three steps. First, we diagonalize the Hamiltonian with and without the NNN interaction in a three-nucleon basis for all relevant three-body channels. In the second step, we use the three-body solutions from the first step to derive three-body effective interactions with and without the NNN interaction. By subtracting the two effective interactions we isolate the NN and NNN contributions. This is needed due to a different scaling with particle's number of the two- and the three-body interactions. The ^{4}He efffective interaction is then obtained by adding the two contributions with the appropriate scaling factors [12]. In the third step, we diagonalize the resulting Hamiltonian in the antisymmetrized four-nucleon Jacobi-coordinate HO basis to obtain the ^{4}He $J^\pi = 0^+0$ ground state. For the LIT calculation we also need the three-body effective interaction for the 1^-1 excited states. Due to the change of parity, both model space size ($N_{\rm max} \to N_{\rm max} + 1$) and effective interaction change. With the effective interactions replacing the interactions in the Hamiltonian (4), the LIT calculation proceeds in steps described in the text following Eq. (4).

We start our discussion presenting the results obtained for the ground state of the α particle based on two different values of the HO parameter, namely $\hbar\Omega = 22$ and 28 MeV. This choice for the HO frequencies is driven by our final goal of evaluating the the ^{4}He photo-absorption

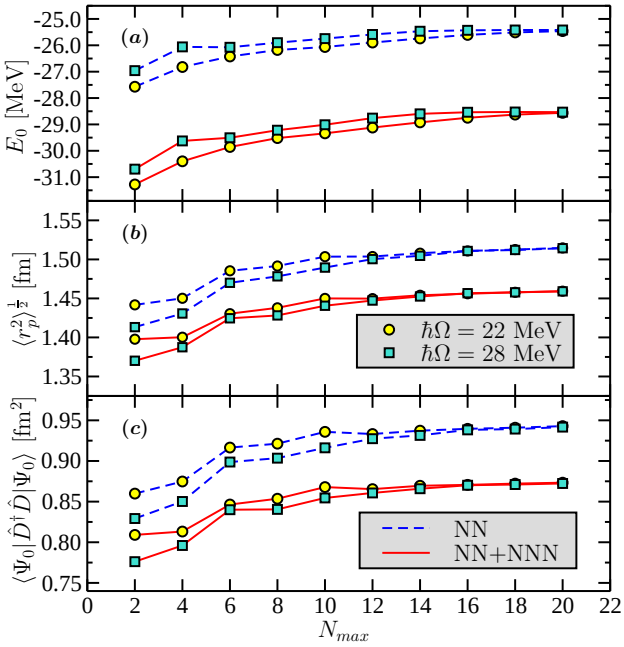

FIG. 1: The ^{4}He ground-state energy E_0 [panel a)], point-proton root-mean-square radius $\langle r_p^2\rangle^{\frac{1}{2}}$ [panel b)] and total dipole strength $\langle\Psi_0|\hat{D}^\dagger\hat{D}|\Psi_0\rangle$ [panel c)] obtained with the χEFT NN and NN+NNN interactions. Convergence pattern with respect to the model space truncation N_{max} for $\hbar\Omega = 22$ and $\hbar\Omega = 28$ MeV.

cross section and related estimate for the theoretical uncertainties. Indeed, in the particular case of the ^{4}He nucleus, frequencies in the range $12 \leq \hbar\Omega \leq 28$ MeV allow to achieve a good description of both ground state and complex energy continuum, required in a calculation of response functions with the LIT method [28].

For all of the three observables examinated in Fig. 1 the χEFT NN and NN+NNN interactions lead to very similar smooth convergence patterns. In particular, an accurate convergence is reached starting from $N_{max} = 18$, as we find independence from both model space and frequency. Although χEFT forces are known to present a relatively soft core, the use of effective interactions for both the NN and NNN interactions is the essential key to this remarkable result. The summary of the extrapolated ground-sate properties is presented in Tab. I. The present results for ground-state energy and point-proton radius with the N^{3}LO NN interaction are consistent with a previous NCSM evaluation ($E_0 = -25.36(4)$ MeV, $\langle r_p^2\rangle^{\frac{1}{2}} = 1.515(10)$ fm) obtained using a two-body effective interaction in a model space up to $N_{max} = 18$ [30] and with that obtained by the hyper-spherical harmonic variational calculation of Ref. [31] ($E_0 = -25.38$ MeV, $\langle r_p^2\rangle^{\frac{1}{2}} = 1.516$ fm) and by the Faddeev-Yakubovsky method [32] ($E_0 = -25.37$ MeV). Finally, with the present choice for the LEC's [10] the calculated binding-energy with inclusion of the NNN force is within few hundred KeV of experiment. This leaves room for additional effects expected from the inclusion of the here missing N^{3}LO NNN (not yet available) and NNNN interaction terms [33].

At the ground-state level, the inclusion of the NNN force affects mostly the energy, providing 3.14 MeV additional binding, while only a weak suppression of about 3.6% is found for the point-proton radius. That the total dipole strength follows the same pattern as the radius and is reduced of 7.4% is not so surprising considering the approximate relation between them [37]:

$$\langle\Psi_0|\hat{D}^\dagger\hat{D}|\Psi_0\rangle \simeq \frac{ZN}{3(A-1)}\langle r_p^2\rangle\,. \qquad (7)$$

The latter expression, which is exact for deuteron and triton and for ground-state wave functions symmetric under exchange of the spatial coordinates of any pair of nucleons, represents a quite reasonable approximation for the α-particle and is found to be about 8% off in our calculations with both the NN and NN+NNN χEFT potentials. As we will see later, this also implies weak NNN effects on the ^{4}He photo-absorption cross section at low energy.

We turn now to the second part of our calculation, for which the ground state is an input. The actual evaluation of Eq. (5) is performed by applying the Lanczos algorithm to the Hamiltonian of the system, using as starting vector $|\varphi_0\rangle = \langle\Psi_0|\hat{D}^\dagger\hat{D}|\Psi_0\rangle^{-\frac{1}{2}}\hat{D}|\Psi_0\rangle$ [24, 28]. Indeed, the LIT can be written as a continued fraction of the elements of the resulting tridiagonal matrix, the so-called Lanczos coefficients a_n and b_n:

$$L(\sigma) = \frac{1}{\sigma_I}\mathrm{Im}\frac{\langle\Psi_0|\hat{D}^\dagger\hat{D}|\Psi_0\rangle}{(z-a_0) - \cfrac{b_1^2}{(z-a_1) - \cfrac{b_2^2}{(z-a_2) - \cfrac{b_3}{\cdots}}}}\,. \qquad (8)$$

Due to the selection rules induced by the dipole operator (3), for a given truncation N_{max} in the 0^+0 model space used to expand the ground state, a complete calculation of Eq. (8) requires an expansion of $|\varphi_0\rangle$ over a 1^-1 space up to $N_{max}+1$. This is the origin of the even/odd notation for N_{max} introduced to describe the convergence of the LIT in Fig. 2.

TABLE I: Calculated ^{4}He ground-state energy E_0, point-proton root-mean-square radius $\langle r_p^2\rangle^{\frac{1}{2}}$, and total dipole strength $\langle\Psi_0|\hat{D}^\dagger\hat{D}|\Psi_0\rangle$ obtained using the χEFT NN and NN+NNN interactions compared to experiment. The experimental value of the point-proton radius is deduced from the measured alpha-particle charge radius, $\langle r_c^2\rangle^{\frac{1}{2}} = 1.673(1)$ fm [34], proton charge radius, $\langle R_p^2\rangle^{\frac{1}{2}} = 0.895(18)$ fm [35], and neutron mean-square-charge radius, $\langle R_n^2\rangle = -0.120(5)$ fm^2 [36].

	E_0 [MeV]	$\langle r_p^2\rangle^{\frac{1}{2}}$ [fm]	$\langle\Psi_0\|\hat{D}^\dagger\hat{D}\|\Psi_0\rangle$ [fm^2]
NN	-25.39(1)	1.515(2)	0.943(1)
NN+NNN	-28.53(2)	1.460(2)	0.874(1)
Expt.	-28.296	1.455(7)	-

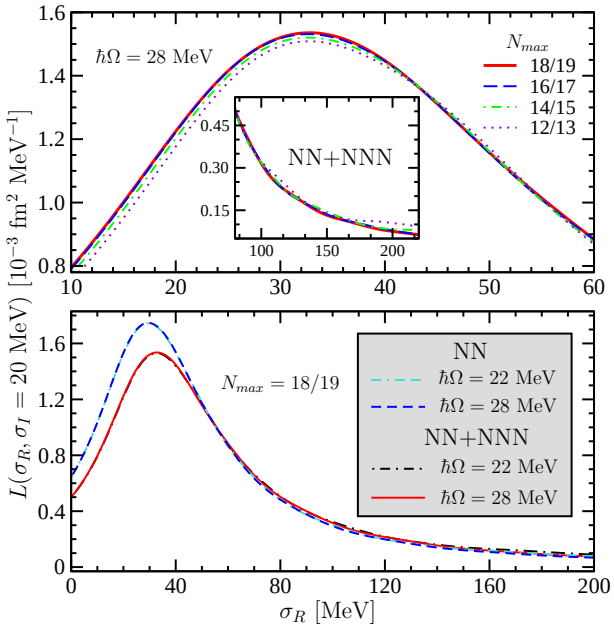

FIG. 2: (Color online) The LIT of the ^{4}He dipole response as a function of σ_R at $\sigma_I = 20$ MeV. Convergence pattern of the NN+NNN calculation with respect to the model-space truncation N_{max} for $\hbar\Omega = 28$ MeV (upper panel), and frequency dependence of the best ($N_{max} = 18/19$) results with and without inclusion of the NNN force (lower panel).

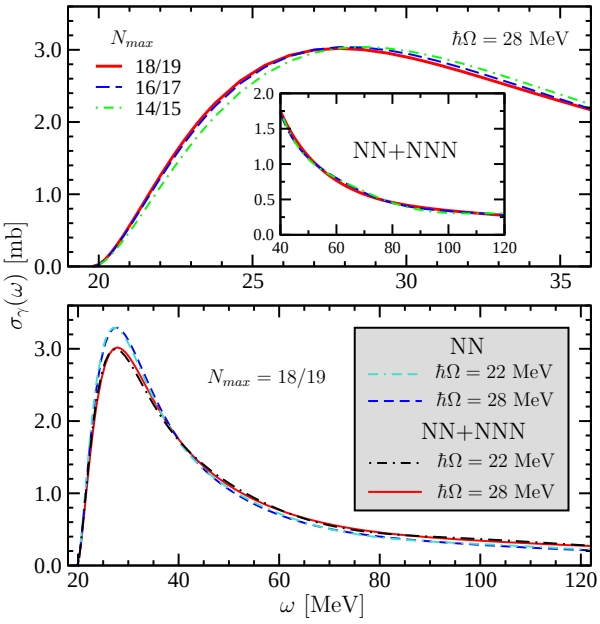

FIG. 3: (Color online) The ^{4}He photo-absorption cross section as a function of the excitation energy ω. Convergence pattern of the NN+NNN calculation with respect to the model-space truncation N_{max} for $\hbar\Omega = 28$ MeV (upper panel), and frequency dependence of the best ($N_{max} = 18/19$) results with and without inclusion of the NNN force (lower panel).

As for the ground-state properties, also the LIT's obtained using the NN and NN+NNN χEFT interactions follow very similar convergence patterns. As an example, in the upper panel of Fig. (2) we show the model-space dependence of the NN+NNN result at $\hbar\Omega = 28$ MeV. Thanks to the use of three-body effective interaction for both the NN and NNN terms of the potential, stable position and height of the peak in the low-σ_R region and satisfactory quenching of the oscillations in the tail are found for $N_{max} = 18/19$. The bottom panel of Fig. 2 indicates that for this model space truncation we find also a fairly good agreement between the $\hbar\Omega = 22$ MeV and $\hbar\Omega = 28$ MeV calculations, in particular below $\sigma_R = 60$ MeV, where for both NN annd NN+NNN interactions the two curves are within 0.5% or less off each other. At higher σ_R the $\hbar\Omega = 22$ MeV results present a weak oscillation (less than 5% in the range 60 MeV $\leq \sigma_R \leq 140$ MeV) around the $\hbar\Omega = 28$ MeV curves, and the discrepancy between the two frequencies becomes larger beyond $\sigma_R = 140$ MeV, where the absolute value of the LIT is small. As we will see later, this small discrepancy will be propagated to the cross section by the inversion procedure [**?**], giving rise to the uncertainty of our calculations. As for the NNN effects at the level of the LIT, the shift of about 3 MeV in the position of the peak is due to the different ground-state energies for the NN and NN+NNN potentials. In addition one can notice a quenching of about 12% of the peak height.

In analogy with Fig. 2, Fig. 3 shows the convergence behavior of our results for the cross section. Starting from $N_{max} = 14/15$ the calculated LIT's are accurate enough to find stable inversions for the response function, and hence deriving the corresponding results for the cross section. The curves obtained for the NN+NNN interaction at the HO frequency value of $\hbar\Omega = 28$ MeV are shown in the upper panel: the model space dependence is weak and the difference between $N_{max} = 16/17$ and 18/19 never exceeds 5% in the range from threshold to $\omega = 120$ MeV. A somewhat larger discrepancy (within 7%) is found by comparing the best results ($N_{max} = 18/19$) for $\hbar\Omega = 22$ MeV and 28 MeV. As for the LIT, the first oscillates slightly around the second. We will use this discrepancy as an estimate for the theoretical uncertainty of our calculations. Note that both the NN and NN+NNN calculated cross sections are translated on the experimental threshold for the ^{4}He photo-disintegration, $E_{th} = 19.8$ MeV ($\omega \to \omega + \Delta E_{th}$, with ΔE_{th} being the difference of the calculated and experimental thresholds). The same procedure will be applied later in the comparison with experimental data and different potential models. Under this arrangement, the position of the peak is not affected by the inclusion of the NNN force, while the relative difference between the NN and NN+NNN cross sections varies almost linearly from -10% at threshold to about $+30\%$ at $\omega = 120$ MeV. In particular, the peak height undergoes a 8% suppression and the two curves cross around $\omega = 40$ MeV. In view of the inverse-energy-

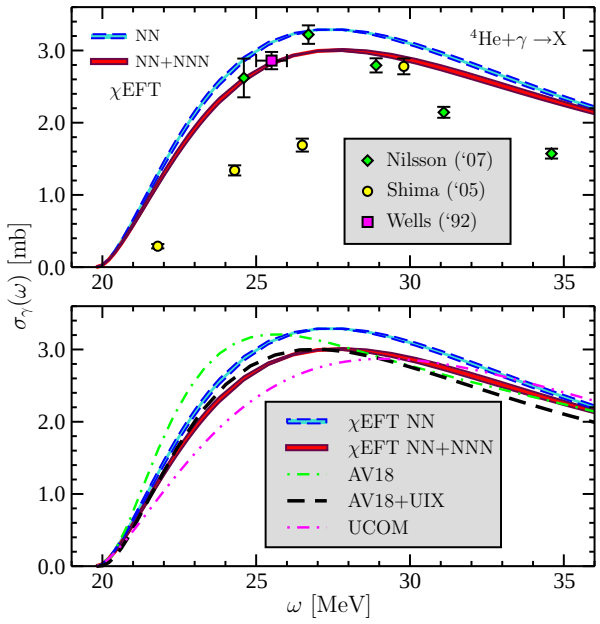

FIG. 4: The ^{4}He photo-absorption cross section as a function of the excitation energy ω. Present NCSM results obtained using the χEFT NN and NN+NNN interactions compared to: (upper panel) the ^{4}He(γ, n) data of Nilsson *et al.* [16] multiplied by a factor of 2, the total cross section measurements of Shima *et al.* [15], the total photo-absorption at the peak derived from Compton scattering via dispersion relations from Wells *et al.* [38]; (lower panel) the EIHH predictions for AV18, AV18+UIX [39] and UCOM [40]. The widths of the χEFT NN and χEFT NN+NNN curves reflect the uncertainties in the calculations (see text).

weighted integral of the cross-section (1),

$$\int_{E_{th}}^{\infty} \frac{\sigma_\gamma(\omega)}{\omega} d\omega = 4\pi^2 \frac{e^2}{\hbar c} \langle \Psi_0 | \hat{D}^\dagger \hat{D} | \Psi_0 \rangle \ , \qquad (9)$$

the weakness of the NNN effects in the peak region is a consequence of the small suppression found for the total dipole strength. Considering in addition the approximate relation (7), we can infer a weak sensitivity with respect to variations of the LEC's in the NNN force, for which we embrace the preferred choice suggested in Ref. [10].

We compare our results with experimental data in the region $\omega < 40$ MeV, where corrections to the unretarded dipole approximation are expected to be negligible. The data sets from Refs. [16] and [15] are chosen here as the latest examples of controversial experiments characterizing the ^{4}He photo-effect since the 80's (see reviews of available data in Refs. [13, 14] and [15]). Note that in the upper panel of Fig. 4, we estimate the total cross section from the ^{4}He(γ, n) measurements (to very good extent ^{4}He$(\gamma, n)^3$He measurements in the energy range considered here, since the contamination due to the ^{4}He$(\gamma, np)d$ cross section is found to be less than 0.1%) of Ref. [16] by assuming $\sigma_\gamma(\omega) \simeq 2\sigma_{\gamma,n}(\omega)$. The latter assumption, which relies on the similarity of the ^{4}He$(\gamma, p)^3$H and ^{4}He$(\gamma, n)^3$He cross sections, is sufficiently safe below the three-body break-up threshold ($\omega = 26.1$ MeV), above which one should add also the contribution of the ^{4}He$(\gamma, np)d$ disintegration channel, and, 2.2 MeV later, also the four-body breakup. Shima *et al.* [15] provide total photo-disintegration data obtained by simultaneous measurements of all the open channels. Finally, we show also an indirect determination of the photo-absorption cross section deduced from elastic photon-scattering on ^{4}He by Wells et al. [38]. We find an overall good agreement with the photo-disintegration data from bremsstralung photons [16], which are consistent with the indirect measurements of Ref. [38], while we reach only the last of the experimental points of Ref. [15].

The lower panel of Fig. 4 compares our present results with the prediction for the ^{4}He photo-absorption cross section obtained in the framework of the EIHH approach [27] using the AV18, AV18+UIX [39] and UCOM [40] interactions. Interestingly, both the results with AV18 and χEFT NN interactions and those with AV18+UIX and χEFT NN+NNN forces show similar peak heights ($\sim$ 3.2 mb and $\sim$ 3.0 mb respectively), but different peak positions (particularly for the first case) with an overall better agreement of the second set of curves. In this regard we notice that the α-particle ground-state properties obtained with AV18+UIX and the χEFT NN+NNN are very close to each other and to experiment. On the contrary, already at the ground-state level the two NN interactions are less alike as the ^{4}He with the AV18 potential is more than 1 MeV less bound than with the N^{3}LO NN potential, while they still yield to the same point-proton radius. A somewhat larger discrepancy is found between the cross sections obtained with the χEFT NN+NNN and UCOM interactions. Beyond $\omega = 80$ MeV, in the range not shown in the Figure, the χEFT NN+NNN force leads to larger values than AV18+UIX and UCOM in the tail of the cross section. Keeping in mind that at such high energies the cross section is small and the uncertainty in our calculation larger, this effect can be related in part to differences in the details and interplay of tensor and spin-orbit forces in the considered interaction models. Furthermore, corrections to the unretarded dipole operator play here a more important role.

In conclusion we summarize our work. We have calculated the total photo-absorption cross section of ^{4}He using the potentials of χEFT at the orders presently available, the NN at N^{3}LO and the NNN at N^{2}LO. The microscopic treatment of the continuum problem was achieved by means of the LIT method, applied within the NCSM approach. Accurate convergence in the NCSM expansions is reached thanks to the use of three-body effective interactions. Our results show a resonant structure that peaks around $\omega = 27.8$ MeV, with a cross section of 3 mb. The NNN force induces a reduction of the peak and an enhancement of the tail of the cross section. The fairly mild NNN effects are far from explaining the low-lying experimental data of Ref. [15] while moderately improve

the agreement of the calculated cross section with the measurements of Nilsson *et. al.* [16]. In view of the overall good agreement between the χEFT NN+NNN and AV18+UIX calculations, the photo-absorption cross section at low energy appears to be more sensitive to change in the α-particle size, than to the details of the spin-orbit component of the NNN interaction. In this regard, a more substantial role of the NNN force can be expected in the photo-disintegration of p-shell nuclei, for which differences in the spin-orbit strength have crucial effects on the spectrum [10, 41]. Finally, the rather contained width of the theoretical band embracing the χEFT NN+NNN, AV18+UIX and UCOM results within 15 MeV from threshold is remarkable compared to the large discrepancies still present among the different experimental data. Hence the urgency for further experimental activity to help clarify the situation.

Acknowledgments

We would like to thank Winfried Leidemann for supplying us with the computer code for the inversion of the LIT. We are also thankful to Giuseppina Orlandini and Sonia Bacca for useful discussions. This work was performed under the auspices of the U. S. Department of Energy by the University of California, Lawrence Livermore National Laboratory under contract No. W-7405-Eng-48. Support from the LDRD contract No. 04–ERD–058 and from U.S. DOE/SC/NP (Work Proposal Number SCW0498) is acknowledged.

[1] S. Weinberg, Physica A **96**, 327 (1979); J. Gasser and H. Leutwyler, Ann. Phys. **158**, 142 (1984); Nucl. Phys. **B250**, 465 (1985).
[2] S. Weinberg, Phys. Lett. B **251**, 288 (1990), nucl. Phys. **B363**, 3 (1991).
[3] V. Bernard, N. Kaiser, and U.-G. Meißner, Int. J. Mod. Phys. E **4**, 193 (1995).
[4] C. Ordonez, L. Ray, and U. van Kolck, Phys. Rev. Lett. **72**, 1982 (1994); U. van Kolck, Prog. Part. Nucl. Phys. **43**, 337 (1999); P. F. Bedaque and U. van Kolck, Ann. Rev. Nucl. Part. Sci. **52**, 339 (2002); E. Epelbaum, Prog. Part. Nucl. Phys. **57**, 654 (2006).
[5] U. van Kolck, Phys. Rev. C **49**, 2932 (1994).
[6] E. Epelbaum, A. Nogga, W. Glöckle, H. Kamada, U.-G. Meißner, and H. Witala, Phys. Rev. C **66**, 064001 (2002).
[7] E. Epelbaum, Phys. Lett. B **639**, 456 (2006).
[8] D. R. Entem and R. Machleidt, Phys. Rev. C **68**, 041001(R) (2003).
[9] A. Nogga, P. Navrátil, B. R. Barrett, and J. P. Vary, Phys. Rev. C **73**, 064002 (2006).
[10] P. Navrátil, V. G. Gueorguiev, J. P. Vary, W. E. Ormand, and A. Nogga (2007).
[11] P. Navrátil, J. P. Vary, and B. R. Barrett, Phys. Rev. Lett. **84**, 5728 (2000); Phys. Rev. C **62**, 054311 (2000).
[12] P. Navrátil and W. E. Ormand, Phys. Rev. Lett. **88**, 152502 (2002); Phys. Rev. C **68** (2003) 034305.
[13] J. R. Calarco, B. L. Berman, and T. W. Donnelly, Phys. Rev. C **27**, 1866 (1983), and references therein.
[14] S. Quaglioni, W. Leidemann, G. Orlandini, N. Barnea, and V. D. Efros, Phys. Rev. C **69**, 044002 (2004), and references therein.
[15] T. Shima, S. Naito, T. Baba, K. Tamura, T. Takahashi, T. Kii, H. Ohgaki, and H. Toyokawa, Phys. Rev. C **72**, 044004 (2005).
[16] B. Nilsson, et al., Phys. Lett. B **625**, 65 (2005); Phys. Rev. C **75** (2007) 014007.
[17] G. Ellerkmann, W. Sandhas, S. A. Sofianos, and H. Fiedeldey, Phys. Rev. C **53**, 2638 (1996).
[18] V. D. Efros, W. Leidemann, and G. Orlandini, Phys. Rev. Lett. **78**, 4015 (1997).
[19] N. Barnea, V. D. Efros, W. Leidemann, and G. Orlandini, Phys. Rev. C **63**, 057002 (2001).
[20] S. C. Pieper, V. R. Pandharipande, R. B. Wiringa, and J. Carlson, Phys. Rev. C **64**, 014001 (2001).
[21] H. Arenhövel and M. Sanzone, Few. Body Syst. Suppl. **3**, 1 (1991).
[22] J. Golak, et al., Nucl. Phys. **A707**, 365 (2002).
[23] V. D. Efros, Yad. Fiz. **41**, 1498 (1985), [Sov. J. Nucl. Phys. **41**, 949 (1985)]; Yad. Fiz. **56 (7)** , 22 (1993) [Phys. At. Nucl. **56**, 869 (1993)]; Yad. Fiz. **62**, 1975 (1999) [Phys. At. Nucl. **62**, 1833 (1999)].
[24] M. A. Marchisio, N. Barnea, W. Leidemann, and G. Orlandini, Few-Body Syst. **33**, 259 (2003).
[25] V. D. Efros, W. Leidemann, and G. Orlandini, Few-Body Syst. **26**, 251 (1999); D. Andreasi, W. Leidemann, C. Reiß, and M. Schwamb, Eur. Phys. J **A24**, 361 (2005).
[26] V. D. Efros, W. Leidemann, and G. Orlandini, Phys. Lett. B **338**, 130 (1994).
[27] N. Barnea, W. Leidemann, and G. Orlandini, Phys. Rev. C **61**, 054001 (2000); Phys. Rev. C **67**, 054003 (2003).
[28] I. Stetcu, et al., Nucl. Phys. **A** (2007), in press, doi:10.1016/j.nuclphysa.2006.12.047.
[29] P. Navrátil, G. P. Kamuntavicius, and B. R. Barrett, Phys. Rev. C **61**, 044001 (2000).
[30] P. Navrátil and E. Caurier, Phys. Rev. C **69**, 014311 (2004).
[31] M. Viviani, L. E. Marcucci, S. Rosati, A. Kievsky, and L. Girlanda, Few-Body Syst. **39**, 159 (2006).
[32] A. Nogga, (private communication).
[33] D. Rozpedzik, et al., Acta Phys.Polon. **B37**, 2889 (2006).
[34] E. Borie and G. A. Rinker, Phys. Rev. A **18**, 324 (1978).
[35] I. Sick, Phys. Lett. B **576**, 62 (2003).
[36] S. Kopecky, P. Riehs, J. A. Harvey, and N. W. Hill, Phys. Rev. Lett. **74**, 2427 (1995); S. Kopecky, J. A. Harvey, N. W. Hill, M. Krenn, M. Pernicka, P. Riehs, and S. Steiner, Phys. Rev. C **56**, 2229 (1997).
[37] L. L. Foldy, Phys. Rev. **107**, 1303 (1957).
[38] D. P. Wells, D. S. Dale, R. A. Eisenstein, F. J. Federspiel, M. A. Lucas, K. E. Mellendorf, A. M. Nathan, and A. E. O'Neill, Phys. Rev. C **46**, 449 (1992).
[39] G. Doron, S. Bacca, N. Barnea, W. Leidemann, and G. Orlandini, Phys. Rev. Lett. **96**, 112301 (2006).
[40] S. Bacca (2007), nucl-th/0612016.
[41] S. Pieper, Nucl. Phys. **A571**, 516 (2005).